Available online at www.sciencedirect.com

ScienceDirect

IFAC PapersOnline CONFERENCE PAPER ARCHIVE

IFAC PapersOnLine 51-24 (2018) 214–220

The Impact of Lithium-Ion Battery Polarising Impedance Modelling on End-of-Discharge Prognosis Accuracy

Christopher P. Ley, * **Marcos E. Orchard** *,**

* *Department of Electrical Engineering, Universidad de Chile, Santiago 837-0451, Chile, (e-mail: info@christopherley.com)*

** *Advanced Mining Technology Center (AMTC), Universidad de Chile, Santiago 837-0451, Chile, (e-mail: morchard@ing.uchile.cl)*

Abstract: In Lithium-Ion batteries, the polarising impedance is an important characteristic that has been shown to be a complex function of, among others, both the state of charge and the demanded current. Therefore within a prognostic framework, which typically solely relies on the a prior modelling of the hidden state evolution, the correct characterisation of the functional surface with respect to state of charge and current impacts the accuracy of the predicted end-of-discharge probability density function. This is important in critical systems that rely solely on the Lithium-Ion as a power source and require an unbiased prediction of the end-of-discharge time. This paper demonstrates how a correctly modelled polarising surface can improve prediction accuracy over the state of the art models found in literature.

Keywords: Signal Processing, Model Identification, Estimation, Prognostics

1. INTRODUCTION

In Lithium-Ion battery monitoring and the subsequent estimation of the State of Charge (SoC), the polarising impedance is an important characteristic that has been shown to be a complex function of, among others, both the SoC and the demanded current. Therefore within a prognostic framework, which typically solely relies on the hidden state evolution model, the correct characterisation of the functional surface with respect to state of charge and current, impacts the accuracy of the predicted end-of-discharge probability mass function (pmf). This is important in critical systems that rely solely on the Lithium-Ion as a power source and require an unbiased prediction of the end-of-discharge time.

The typical solution to this problem in literature, such as in Quintero et al. (2017); Acuña and Orchard (2017a), is augment the state evolution of the SoC to include an additional state that represents the polarising impedance. This state evolves through a combination of outer-feedback loops, simulated annealing and the re-sampling of the Particle Filter observer to converge on the *current* value of the polarising impedance.

The problem with this approach arises when you consider a scenario where the usage profile constantly changes (a very real scenario), which, inhibits the convergence of this second *artificial evolution* (AE) state. This is due to, as demonstrated for example in Burgos-Mellado et al. (2016), that in fact the polarising impedance is a multidimensional surface which is both a function of current and SoC.

In the following sections, it is shown, how the standard state of the art model struggles in this real world scenario to produce consistent & accurate predictions, regardless of hyper-parameter tuning and how by replacing the polarising impedance AE state with a reproducing kernel significantly improves prognosis accuracy, as well as algorithmic stability.

2. POLARISING IMPEDANCE IN LI-ION BATTERY MODELLING

The state space modelling (SSM) used in battery monitoring are often based of on a simplified equivalent circuit model (ECM)Waag et al. (2013), such as the one depicted in Fig. 1. ECMs are used as their name suggests as an equivalence, as well as a simplification of, the underlying mechanism of ion transfer, kinetics and subsequent Red-Ox reactions within the Lithium-ion battery. ECMs are effective due to their significantly reduced computational complexity compared to a complete model of Lithium-ion kinetics as well as reducing the dependency of the model on parameterisation. The dependence of the ECM performance on correct parameterisation is reduced, but not eliminated, in fact it obscures one of the main difficulties in Lithium-ion battery inference, state varying parameters, specifically the polarising impedance.

In order to understand the problem we will focus on the equivalent model shown in Fig. 1, under this equivalence the resistance $R(I_R)$ can be described by the Butler-Volmer equation (1) Waag et al. (2013):

$$R(I_R) = R_1 \cdot \left(\frac{\ln(k_I \cdot I_R + \sqrt{(k_I \cdot I_k)^2 + 1})}{k_I \cdot I_k} \right) \quad (1)$$

where R_1 is the resistance at $I_R = 0A$ and k_I is a parameter that describes the current dependency of the resistance. It appears as though the resistance varies

2405-8963 © 2018, IFAC (International Federation of Automatic Control) Hosting by Elsevier Ltd. All rights reserved.
Peer review under responsibility of International Federation of Automatic Control.
10.1016/j.ifacol.2018.09.580

depending on the users demand of the battery, but the problem becomes more complex when it can be shown that both parameters (R_1 and k_I) vary with different temperatures (T), States of Health (SoH) and States of Charge (SoC) Burgos-Mellado et al. (2016). So if we were

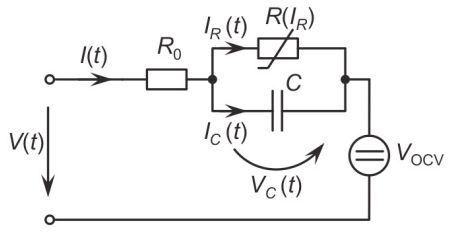

Fig. 1. Example of an Equivalent circuit model (ECM), The voltage source V_{OCV} represents the open circuit voltage (OCV) of the battery, the resistance R_0 corresponds to the internal resistance of the battery at high frequencies, the resistance $R(I_R)$ corresponds mainly to the charge transfer reaction and is current dependency, the capacitance C corresponds to the double layer capacity of the battery.

to express generally a lumped parameter model for the impedance (R_0,$R(I_R)$ & C) we would be considering a highly non-linear model which can be expressed as

$$Z_p = f(SoC, I, SoH, T). \tag{2}$$

which we will call the general polarising impedance model.

3. GENERAL STATE SPACE MODELLING OF LITHIUM-ION BATTERY

The State of Charge (SoC) is an abstract construct that represent an important indicator for estimating the autonomy Orchard et al. (2012) of a battery. The SoC represents a "fuel gauge" of the battery, so naturally we desire a function that

$$\sup SoC \mapsto E_{crit}$$
$$\inf SoC \mapsto 0$$

where E_{crit} is the maximum amount of *energy* ($Watt \cdot hour$) the battery is *currently* capable of containing. Therefore if we consider our ECM (Fig. 1) we can express the rate of change of the SoC as the rate of change in power, the product of the demanded battery current I and observed voltage V, with respect to time as some fraction of our total battery energy E_{crit}:

$$\frac{dSoC}{dt} = \frac{d}{dt}\left(\frac{I \cdot V_t}{E_{crit}}\right). \tag{3}$$

For the sake of simplicity we will adopt a positive power convention where a positive current $I > 0$ represents a *decrease* in energy of our battery, with this in mind we can further discretise (3) with respect to time t, which leaves us with a SSM for SoC in the form:

$$SoC_{k+1} = SoC_k - \frac{\Delta t \cdot I_k \cdot V_k}{E_{crit}} \tag{4}$$

where Δt is unit of discretisation in this context called our "sample time". Now we have defined how the SoC evolves as a function of our control variable I_k and the internal state SoC, we need to define how those two states affect the output voltage, which is included in our model. In order to do so we must consider our equivalent circuit Fig. 1 or its functional equivalency

$$V_k = V_{OCV}(SoC_k) - I_k \cdot Z_p \tag{5}$$

where V_{OCV} is the open circuit voltage (OCV) and is modelled as

$$\begin{aligned} VoC(SoC) = {} & v_L + (v_0 - v_L) \cdot e^{\gamma \cdot (SoC(k)-1)} \\ & + \alpha \cdot v_L \cdot (SoC(k) - 1) \\ & + (1-\alpha) \cdot v_L \cdot \left(e^{-\beta} - e^{-\beta\sqrt{SoC(k)}}\right) \end{aligned} \tag{6}$$

where (α, β, γ) are fixed parameters that are determined initially from battery tests (see Pola et al. (2015) for a rigorous explanation) and form an integral part of the characteristic curve. It is apparent the implication that the accuracy of Z_p is of significance as it directly impacts the accuracy of estimation of the SoC and subsequently its prediction.

4. THE PARTICLE FILTER

All estimation within this paper is performed via the Particle Filter (PF) observer framework, the PF is defined as follows.

Consider a sequence of probability distributions $\pi_t(x)_{t\geq 1}$, where it is assumed that $\pi_t(x_{0:t})$ can be evaluated point-wise up to a normalising constant. Particle Filters (PF) are a class of algorithms designed to approximately obtain samples sequentially from $\{\pi_t\}$ to generate a collection of $N \gg 1$ weighted random samples $\{w_t^{(i)}, x_{0:t}^{(i)}\}_{i=1,\dots,N}, w_t^{(i)} \geq 0, \forall t \geq 1$, satisfying Andrieu et al. (2001):

$$\sum_{i=1}^{N} w_t^{(i)} \varphi_t\left(x_{0:t}^{(i)}\right) \xrightarrow[N\to\infty]{} \int \varphi_t(x_{0:t}) \pi_t(x_{0:t}) dx_{0:t}, \tag{7}$$

where φ_t is any π_t-integrable function. In the particular case of the Bayesian Filtering problem, the *target distribution* $\pi_t(x_{0:t}) = p(x_{0:t}|y_{1:t})$ is the *posterior* pdf of $X_{0:t}$, given a realisation of noisy observations $Y_{1:t} = y_{1:t}$. In a Bayesian filtering observer framework we define the general state evolution

$$p(x_k|x_{k-1}) \approx f(x_k|x_{k-1}) \tag{8}$$

and the general observation

$$p(y_k|x_k) \approx g(y_k|x_k) \tag{9}$$

where x_k is the hidden state at instance k, such as the SoC_k in (4), and y_k is the observation at instance k, e.g. V_k in (5).

Using (8) and (9), $\pi_t(x_{0:t})$ may be written as Doucet et al. (2001)

$$\pi_t(x_{0:t}) = p(x_0) \prod_{k=1}^{t} f_k(x_k|x_{k-1}) g_k(y_k|x_k) \tag{10}$$

Let a set of N paths $\{x_{0:t-1}^{(i)}\}_{i=1,\dots,N}$ be available at time $t-1$. Furthermore, let these paths distribute according to $q_{t-1}(x_{0:t-1})$, also referred to as the *importance* density function at time $t-1$. Then, the objective is to efficiently obtain a set of N new paths (particles) $\{\tilde{x}_{0:t}^{(i)}\}_{i=1,\dots,N}$ approximately distributed according to $\pi(\tilde{x}_{0:t})$ Andrieu et al. (2001).

For this purpose, the current paths $x_{0:t-1}^{(i)}$ are extended by using the kernel $q_t(\tilde{x}_{0:t}|x_{0:t-1}) = \delta(\tilde{x}_{0:t-1} - x_{0:t-1}) \cdot q_t(\tilde{x}_t|x_{0:t-1})$, ie, $\tilde{x}_{0:t} = (x_{0:t-1}, \tilde{x}_t)$. The *importance sampling* procedure generates consistent estimates for the expectation by approximating (10) with the empirical distribution Andrieu et al. (2001)

$$\tilde{x}_t^N(x_{0:t}) = \sum_{i=1}^{N} w_{0:t}^{(i)} \delta\left(x_{0:t} - \tilde{x}_{0:t}^{(i)}\right) \tag{11}$$

where $w_{0:t}^{(i)} \propto w_{0:t}(\tilde{x}_{0:t}^{(i)})$ and $\sum_{i=1}^{N} w_{0:t}^{(i)} = 1$.

4.1 Sequential Importance Sampling/Resampling Particle Filter (SIR-PF)

The simplest PF implementation - the SIS particle filter - computes the value of the particle weights $w_{0:t}^{(i)}$, by setting the importance density function equal to *a priori* pdf for the state, ie, $q_t(\tilde{x}_{0:t}|x_{0:t-1}) = p(\tilde{x}_t|x_{t-1}) = f_t(\tilde{x}_t|x_{t-1})$. In that manner, the weights for the newly generated particles are evaluated from the likelihood of new observations. The efficiency of the procedure improves as the variance of the importance weights is minimized. The choice of the importance density function is critical for the performance of the particle filter scheme and hence, it should be considered in the filter design.

One of the main difficulties that must be addressed in the implementation of SIS particle filters is the problem of *particle degeneracy* Doucet et al. (2001) since, after a few iterations, all but one particle could have a negligible weight Andrieu et al. (2001); Doucet et al. (2001). Several methods have been proposed to overcome this problem, one of which is to perform the re-sampling procedure conditionally on a test of the *Effective Sampling Size* (N_{eff}) criterion, given by Li et al. (2014):

$$N_{eff} = \left(\sum_{i=1}^{N} \left(\omega_t^{(i)}\right)^2\right)^{-1} \quad \text{s.t.} \quad \sum_{i=1}^{N} \omega_t^{(i)} = 1 \tag{12}$$

The re-sampling is only implemented when the N_{eff} is below a threshold N_T, e.g. $N_T = 0.85 * N$, where N is the size of the particle population. This process avoids *sample impoverishment* and permits the Particle Filter to converge to the optimal filter, in the weak sense, with the rate of $1/\sqrt{N}$. The SIS in combination with the re-sampling step is referred to as the Sequential Importance Sampling Resampling (SIR) Particle Filter, full details of which can be found in Doucet and Johansen (2011).

5. PARTICLE-FILTERING BASED PROGNOSIS

It is possible to describe the evolution in time of the degradation of the non-linear state equations used in the estimation phase (Sec. 4). By using the state equation (8), it is possible to generate long-term predictions using kernel functions to reconstruct the estimate of the state probability density function (pdf) in future time instants.

The goal is to produce a predicted conditional state pdf $\hat{p}(x_{t+k}^{(i)}|\hat{x}_{t+k-1}^{(i)})$, which describes the state distribution at the future time instant $t+k, (k = 1, \ldots, \rho)$ when the particle $\hat{x}_{t+k-1}^{(i)}$ is used as an initial condition. Assuming that the current weights $\{w_t^{(i)}\}_{i=1,\ldots,N}$ are a good representation of the state pdf at time $t+k$, by using the law of total probabilities and the particle weights at time $t+k-1$, as shown in (13)

$$\begin{aligned} \hat{p}(x_{t+k}|\hat{x}_{1:t+k-1}) &\approx \sum_{i=1}^{N} w_{t+k-1}^{(i)} \cdot \hat{p}(x_{t+k}^{(i)}|\hat{x}_{t+k-1}^{(i)}), \\ \hat{x}_t^{(i)} &= \tilde{x}_t^{(i)}, \qquad k = 1, \ldots, \rho \end{aligned} \tag{13}$$

To evaluate (13), the weight of every particle should be modified (at each prediction step) to take into account the fact that noise and process non-linearities could change the shape of the state pdf as time passes. However, since the weight update procedure is needed as part of a prediction problem, it cannot depend on the acquisition of new measurements. Additionally, before proceeding with the next prediction step, it is necessary to allocate a new set of particles within the domain of the probability distribution (13). To overcome most of these difficulties Orchard and Vachtsevanos (2009) proposed a method of using a kernel to represent the uncertainty growth of each prediction step.

Consider a discrete approximation (14) for the predicted state pdf (13), where $K(\cdot)$ is a kernel density function, which may correspond to the process noise pdf, a Gaussian Kernel or a re-scaled Epanechnikov Kernel Orchard and Vachtsevanos (2009).

$$\hat{p}(x_{t+k}|\hat{x}_{1:t+k-1}) \approx \sum_{i=1}^{N} \omega_{t+k-1}^{(i)} K\left(x_{t+k} - E\left[x_{t+k}^{(i)}|\hat{x}_{t+k-1}^{(i)}\right]\right) \tag{14}$$

The kernel method utilised is a modified version of the *Regularised Particle Filter* presented by Musso et al. (2001), where they present an optimum re-scaled Epanechnikov kernel, given by:

$$\begin{aligned} A &= \left(8c_{n_x}^{-1}(n_x+4)(2\sqrt{\pi})^{n_x}\right)^{1/(n_x+4)} \\ h_{opt} &= A \cdot N^{-1/(n_x+4)} \\ K_h &= \frac{1}{h^{n_x}} K\left(\frac{x}{h}\right) \end{aligned} \tag{15}$$

$$K(x) = \begin{cases} \dfrac{n_x+2}{2c_{n_x}}\left(1 - \|x\|^2\right) & \text{if } \|x\| < 1 \\ 0 & \text{otherwise} \end{cases}$$

where c_{n_x} is the volume of the unit sphere in $\mathbb{R}^{n_x}$. Rather than simply projecting the expectation of the state variables into the future, the uncertainty of (14) can be represented by generating a population of equally weighted particles at time instant $t+k$, $1 \le k \le \rho$, and performing an inverse transform re-sampling procedure for the particle population. The focus is to represent the growth of uncertainty presented in (14). For that, samples distributed according to (14) are obtained by selecting $u^{(i)} = i \cdot (N+1)^{-1}$ for $i : 1, \cdots, N$ and interpolating a value for $\hat{x}_{t+k}^{(i)}$ from the cumulative state distribution

$$F(X_{t+k} \le x_{t+k}) = \int_{-\infty}^{x_{t+k}} \hat{p}(x_{t+k}|\hat{x}_{1:t+k-1}) dx_{t+k} \tag{16}$$

in accordance with $\hat{x}_{t+k}^{(i)} = F^{-1}(u^{(i)})$. Considering all of the above, the regularisation algorithm Musso et al. (2001) is used to perform prognosis by Orchard and Vachtsevanos (2009):

(1) Apply modified inverse transform re-sampling procedure for $i = 1, \cdots, N$, where $\omega_{t+k}^{(i)} = N^{-1}$
(2) Calculate $\hat{S}_{t+k}$, the empirical co-variance matrix of
$$\left\{ E\left[x_{t+k}^{(i)} | \hat{x}_{t+k-1}^{(i)} \right], \omega_{t+k}^{(i)} \right\}_{i=1}^{N} \tag{17}$$
(3) Compute $\hat{D}_{t+k}$ such that $\hat{D}_{t+k}\hat{D}_{t+k}^{T} = \hat{S}_{t+k}$
(4) For $i = 1, \cdots, N$, draw $\epsilon^{i} \sim K$, the Epanechnikov kernel and assign $\hat{x}_{t+k}^{(i)*} = \hat{x}_{t+k}^{(i)} + h_{t+k}^{opt}\hat{D}_{t+k}\epsilon^{i}$ where h_{t+k}^{opt} is calculated as in (15) and $\hat{x}_{t+k}^{(i)*}$ is the regularised particle population.
5* For the next prediction step $\hat{x}_{t+k-1}^{(i)*} = \hat{x}_{t+k-1}^{(i)}$

It is assumed that the state co-variance matrix $\hat{S}_{t+k}$ is equal to the empirical co-variance of $\hat{x}_{t+k}$ and that a set of equally weighted samples for $\hat{x}_{t+k-1}$ is available. This serves to maximise the efficiency of the Epanechnikov Kernel.

6. CALCULATING THE PROBABILITY MASS FUNCTION OF THE END OF DISCHARGE

Using the Particle Filter based Prognosis framework outline in Sec. 5, a projection of the evolution of the state probability density function is produced for all time $k > k_p$, where k_p is the prognosis start point. In the case of battery State of Charge (SoC) prediction this is only informative in limited sense. Often the desired prediction in practice is not the probability of state with respect to time but, given a desired limit (of SoC), what is the probability we will reach the limit with respect to time.

In battery prognosis often the limit is referred to as the End-of-Discharge (EoD) point, in the case of this paper is set as $EoD \triangleq SoC \leq 0.3$ or $EoD = 0.3$ is the out limiting point. Acuña and Orchard (2017a) outlines how to calculate the probability mass function with respect to time, described as

$$\mathcal{P}(EoD = 0.3) = \sum_{i=1}^{N_p} W_k^{(i)} p(EoD | SoC_k^{(i)}) \tag{18}$$

which involves summing the projected state trajectories with respect to time at the instance the particle $SoC_{k_p:k}^{(i)} \leq EoD$ in order to accumulate samples from the projected PMF, the process is thoroughly described in Acuña and Orchard (2017a).

7. TESTING PROFILE

With the observation and subsequent prognosis framework defined in Sec. 4 & 5, we will focus on the application case. In this paper we will be using a profile developed from the battery data found in Burgos-Mellado et al. (2016), whose specifications can be found in Appendix A and whose profile is demonstrated in Fig. 2.

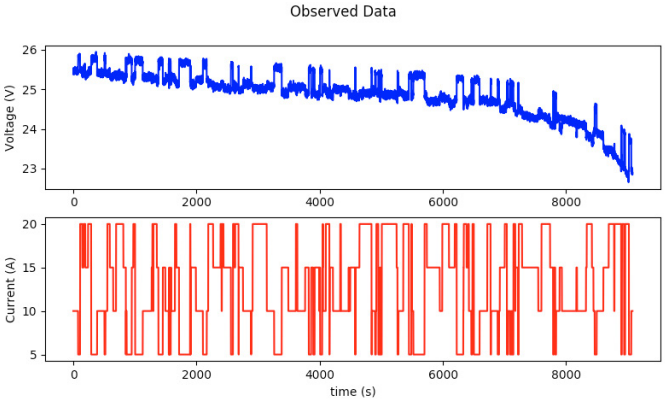

Fig. 2. Lithium-Ion Battery Validation Profile

8. STATE OF THE ART STANDARD MODEL

As it was alluded to in Sec. 1 the state of the art state space model (SSM) in Lithium-Ion battery State of Charge estimation and prognosis, such as the one found in Quintero et al. (2017), consists of defining an additional artificial evolution state that represents a constantly evolving Z_{pol} in order to resolve the observation and state equations dependence on (5), which includes Z_{pol}. This is defined by the random walk model

$$Z_{pol}(k) = Z_{pol}(k-1) + \eta_k \tag{19}$$

where η_k is artificially augmented noise model that is modified through simulated annealing and outer-feedback correction loops (see Orchard et al. (2009) for more details) in order to produce convergence, essentially *learning* the polarising impedance through observations. The state of charge evolution is generally defined by

$$SoC_{k+1} = SoC_k - \frac{\Delta t \cdot I_k \cdot V_k}{E_{crit}} + \omega_k \tag{20}$$

where ω_k represents the state evolution uncertainty generally modelled as zero mean i.i.d Gaussian noise modelled as $\mathcal{N}(0, \sigma_\omega^2)$ for simplicity. The observations are modelled by the equation

$$V_k = V_{OCV}(SoC_k) - I_k \cdot Z_p + \nu_k \tag{21}$$

where ν_k is zero mean i.i.d Gaussian noise generally modelled as $\mathcal{N}(0, \sigma_\nu^2)$.

8.1 Estimation and Prediction Results

As it has already been mentioned this convergence can be hindered by a profile such as the one used in Fig. 2. The result is a model that is constantly correcting during the estimation phase as we can see in Fig. 3 & Fig. 4.

It is often left unsaid that the performance of the particle filter (PF) in the case of the standard model (19), (20), and (21) is often heavily dependent on the hyper-parameter tuning, specifically $\sigma_\omega, \sigma_\nu, \eta$ and their relative sizes. Fig. 3 & Fig. 4 are examples of two extreme cases of this reality.

Fig. 3 represents the situation where the user wishes force the algorithm to actually converge, which can be achieved by decreasing σ_ω and increasing σ_ν, effectively biasing the PF to favour the a prior state model (20) over any observed differences from measurements. This results in a case where the model is artificially confident in it's estimation of the state and subsequently the polarising impedance

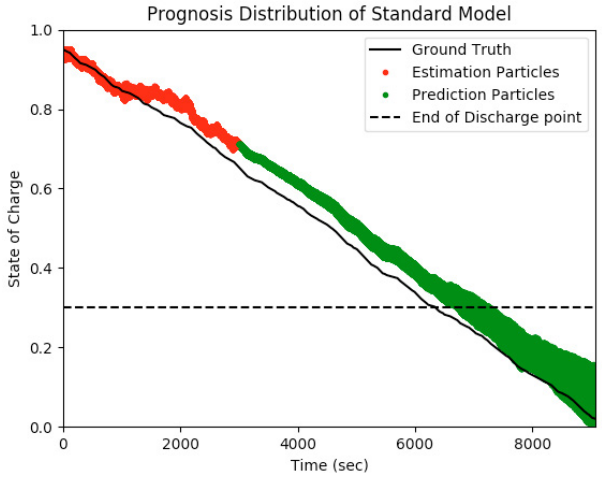

Fig. 3. Artificially high precision in prognosis

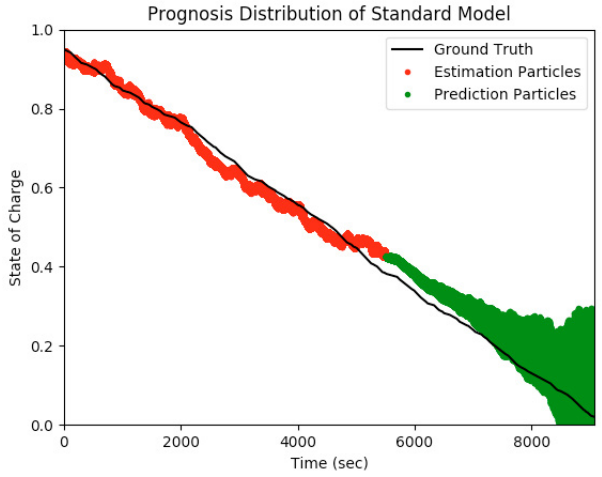

Fig. 4. Better Estimation but low prediction precision - A much more honest model

(19) converges. This can be easily observed in Fig 3 as it can be seen that the model is biased away from the ground truth and has failed to correct. The result of this is in prognosis, as has been detailed in Acuña and Orchard (2017b), is that the predicted probability mass function (PMF, described in Sec. 6) is artificially narrow which is not an accurate representation of the *true* precision of the algorithm. This affect can be further demonstrated by inspecting how the predicted PMF varies at all stages of the estimation. Fig. 5 shows how the mean and variance of the prediction PMF varies at all prognosis starting times for an estimation of when the $SoC = 0.3$. The blue line represents the predicted PMF mean and the shaded area, the variance. Initially the variance of the predicted PMF is reasonable, but as the estimation is allowed to proceed, the AE state converges and produces highly biased artificially confident results (shown by the thin shaded areas). The highly biased results shown in Fig. 5 can be understood by considering the underlying profile to be used during estimation (Fig. 2), depending on where the estimation stops will depend on where in the polarising surface the AE will converge, and subsequently use uncorrected in prognosis.

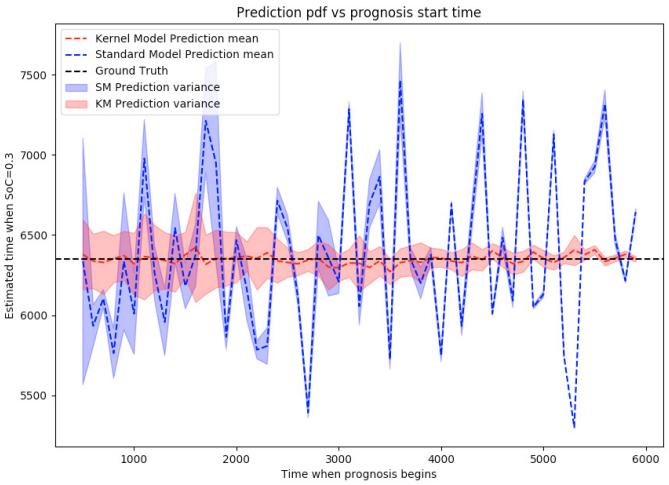

Fig. 5. Prognosis probability density function evolution of model used in 3

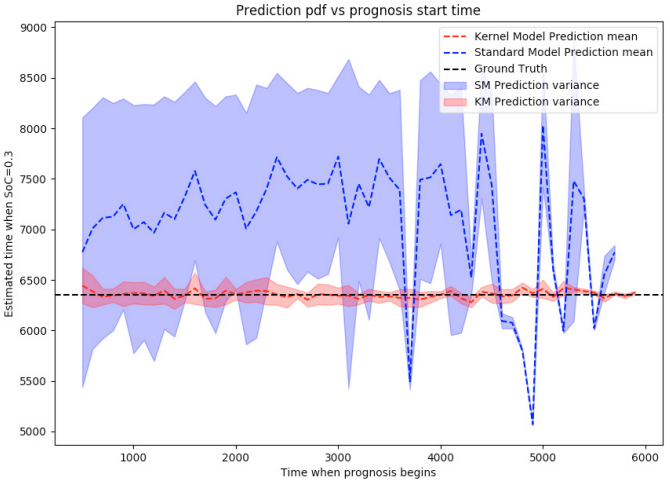

Fig. 6. Prognosis density function evolution of model using in 4

The second situation, shown in Fig. 4, is a pessimistic model that understands the poor modelling capability of a single dimension polarising impedance. This is represented by a hyper-parameter tuning that increases σ_ω and uses the measured σ_ν (or the true measurement uncertainty). This results in significantly improved estimation accuracy, as shown in Fig. 4 by the estimation constantly correcting to close to the true SoC. The consequence of this tuning is that, due to the constantly changing profile, that the AE state never converges. This, in turn, during the prognosis stage creates a large uncertainty (from the large variance in Z_{pol}). It can be seen in Fig. 6 that this is almost invariant of the starting point (up to the point the estimation is very close to the prediction point). Despite a large prediction uncertainty it is mostly stable, although not very accurate.

In a broad sense the competing philosophies of these two models highlight two important factors that should be incorporated in an accurate model,

(1) for estimation accuracy a large range of values is required for the polarising impedance
(2) for accurate prognosis low state uncertainty is required

these two competing ideals in the standard model can be incorporated into one model if we instead consider a polarising surface.

9. KERNEL STATE SPACE MODEL

By refactoring (21) to include $Z_{pol} \approx f(SoC_k, I_k)$ as

$$V_k = VoC_k(SoC_k) - I_k \cdot Z_{pol}(SoC_k, I_k) + \nu_k \tag{22}$$

we can consider $f(SoC_k, I_k)$ as a non-linear surface, this suggests that we could approximate said surface in the reproducing kernel Hilbert space (RKHS) $\mathcal{H}$ with reproducing kernel K.

According to the representer theorem Tobar et al. (2015), the optimal estimate with respect to an arbitrary loss function can be expressed in terms of the kernel function K, input training samples x_i and a vector of mixing parameters $\mathbf{a} = [a_i, \ldots, a_N]$ in the form

$$Z_{pol} = \sum_{i=1}^{N_a} a_i K((SoC_k, I_k), \mathbf{s}_i) \tag{23}$$

where the centres of the kernel evaluations are referred to as *support vectors*. The Gaussian Kernel is defined

$$K(x_i, x_j) = \exp\left(\frac{-\|x_i - x_j\|^2}{\sigma_K^2}\right) \tag{24}$$

where x_i, x_j are the input vectors and the parameter $\sigma_K > 0$ is the kernel width.

9.1 Application to estimation and Prognosis

The kernel was learnt from a previous set of discharge tests of the same battery using a Particle Markov Chain Monte Carlo algorithm to infer the joint probability $p(SoC_{0:T}, \boldsymbol{\theta}|V_{0:T})$, where $\boldsymbol{\theta} = [a_0, \ldots, a_{N_a}, \sigma_\omega]$ (details of which will be outlined in a future publication). The surface can be seen to be highly nonlinear with respect to both SoC and I as can be seen from the plot of level curves of the surface in Fig. 7.

The result of incorporating the learnt surface into the estimation and prognosis stage can be seen firstly in Fig. 8. It can be seen that the estimation incorporates the state uncertainty correctly (as it was part of the learning paradigm) and performs consistently regardless of the usage profile. Fig. 5 and Fig. 6 demonstrate the unbiased correctly confident prediction results (shown in red). It is important to note that the model correctly incorporates in its prediction results correct entropy growth, i.e. the further the prediction is from the estimated PMF, the greater the uncertainty, accurately representing reality.

Further more if we plot the results of one of the commonly used precision metric, such as the Online Precision Index Ley and Orchard (2017)

$$I_k = exp\left(-\frac{|\inf(EoD) - \sup(EoD)|}{|\mathbb{E}[EoD] - t|}\right) \tag{25}$$

where EoD is the PMF of the desired End-of-Discharge estimate (e.g $EoD = 0.3$ in the case of this paper), we can see that in Fig. 9 that the Kernel Model is almost always an improvement on even the most precise standard model.

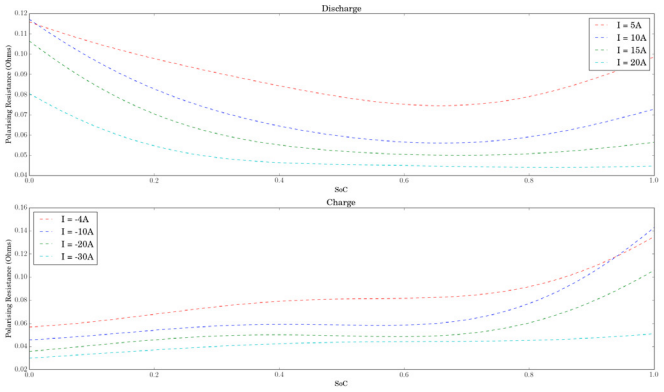

Fig. 7. Level curves from the learnt polarising surface

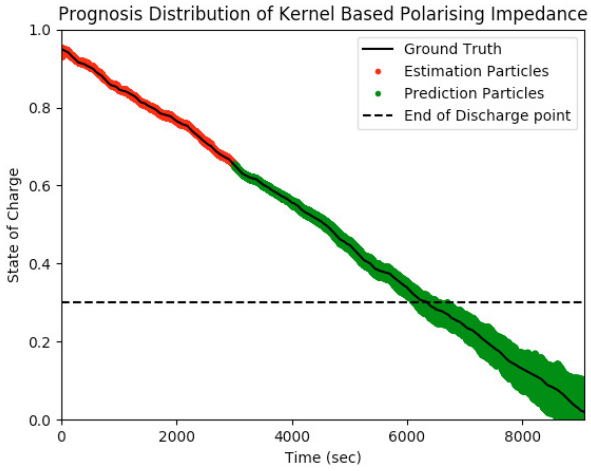

Fig. 8. Prediction evolution of Kernel Based Model

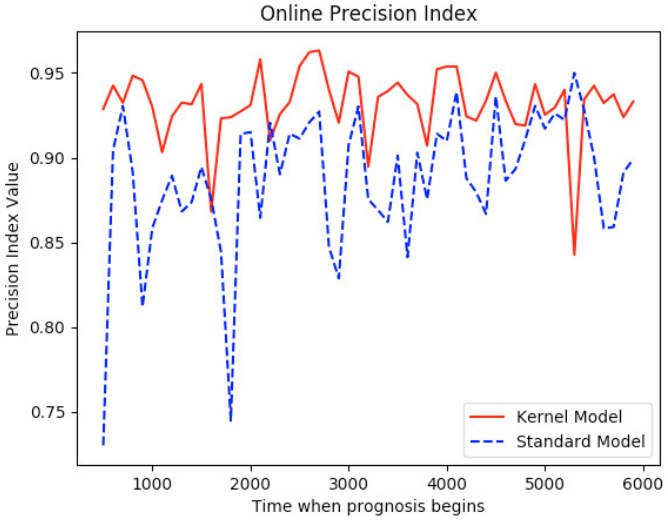

Fig. 9. Precison Index of Kernel Model vs the artificially precise Standard Model, still shows an improvement

10. CONCLUSION

It can be seen that in all presented cases the correct modelling of the polarising impedance surface is always an improvement on the performance of the standard model that is used in the state of the art. This is due to the fact that the kernel model leads to a more informed estimation

model which, leads to a smaller estimation uncertainty and subsequently a reduced initial uncertainty (for the prediction evolution). This can easily be reasoned theoretically due to an increase in the information contained in the model, reduces the Shannon entropy contributed by the state model.

This leads naturally to an emphasis on the importance of the proposed future work of demonstrating a Particle Markov Chain Monte Carlo method for learning the polarising impedance kernel weights.

REFERENCES

Acuña, D.E. and Orchard, M.E. (2017a). Particle-filtering-based failure prognosis via sigma-points: Application to Lithium-Ion battery State-of-Charge monitoring. *Mechanical Systems and Signal Processing*, 85, 827–848.

Acuña, D.E. and Orchard, M.E. (2017b). Prognostic Algorithms Design Based on Predictive Bayesian Cramér-Rao Lower Bounds. *IFAC-PapersOnLine*, 50(1), 4719–4726.

Andrieu, C., Doucet, A., and Punskaya, E. (2001). Sequential Monte Carlo methods for optimal filtering. In *Sequential Monte Carlo Methods in Practice*, 79–95. Springer.

Burgos-Mellado, C., Orchard, M.E., Kazerani, M., Cárdenas, R., and Sáez, D. (2016). Particle-filtering-based estimation of maximum available power state in lithium-ion batteries. *Applied Energy*, 161, 349–363.

Doucet, A., De Freitas, N., and Gordon, N. (2001). *Sequential Monte Carlo methods in practice*. Springer.

Doucet, A. and Johansen, A.M. (2011). A tutorial on particle filtering and smoothing: Fifteen years later. *Handbook of nonlinear filtering*, 12(656-704), 3.

Ley, C.P. and Orchard, M.E. (2017). Chi-squared smoothed adaptive particle-filtering based prognosis. *Mechanical Systems and Signal Processing*, 82, 148–165.

Li, T., Sun, S., Sattar, T.P., and Corchado, J.M. (2014). Fight sample degeneracy and impoverishment in particle filters: A review of intelligent approaches. *Expert Systems With Applications*, 41(8), 3944–3954.

Musso, C., Oudjane, N., and Le Gland, F. (2001). Improving regularised particle filters. In *Sequential Monte Carlo methods in practice*, 247–271. Springer.

Orchard, M., Tobar, F., and Vachtsevanos, G. (2009). Outer feedback correction loops in particle filtering-based prognostic algorithms: Statistical performance comparison. *Studies in Informatics and Control*, 18(4), 295–304.

Orchard, M.E., Cerda, M.A., Olivares, B.E., and Silva, J.F. (2012). Sequential monte carlo methods for discharge time prognosis in lithium-ion batteries. *International Journal of Prognostics and Health Management Volume 3 (color)*, 90.

Orchard, M.E. and Vachtsevanos, G.J. (2009). A particle-filtering approach for on-line fault diagnosis and failure prognosis. *Transactions of the Institute of Measurement and Control*.

Pola, D.A., Navarrete, H.F., Orchard, M.E., Rabié, R.S., Cerda, M.A., Olivares, B.E., Silva, J.F., Espinoza, P.A., and Pérez, A. (2015). Particle-Filtering-Based Discharge Time Prognosis for Lithium-Ion Batteries With a Statistical Characterization of Use Profiles. *IEEE Transactions on Reliability*, 64(2), 710–720.

Quintero, V., Estevez, C., and Orchard, M. (2017). State-of-charge estimation to improve energy conservation and extend battery life of wireless sensor network nodes. In *Ubiquitous and Future Networks (ICUFN), 2017 Ninth International Conference on*, 153–158. IEEE.

Tobar, F., Djurić, P.M., and Mandic, D.P. (2015). Unsupervised state-space modeling using reproducing kernels. *IEEE Transactions on Signal Processing*, 63(19), 5210–5221.

Waag, W., Fleischer, C., and Sauer, D.U. (2013). On-line estimation of lithium-ion battery impedance parameters using a novel varied-parameters approach. *Journal of Power Sources*, 237, 260–269.

Appendix A. BATTERY MODEL PARAMETRISATION

Battery Parameter	$\mathbf{I \geq 0}$	$\mathbf{I < 0}$
Nominal Capacity	40 $A \cdot h$	
Nominal Voltage	25.6 V	
E_{crit}	3133440.0	
v_L	1.0	0.98345
v_0	26.792	26.750
γ	0.556	
α	-2.631	-2.733
β	0.508	0.567
ω_k	$\mathcal{N}(0, 0.001^2)$	
ν_k	$\mathcal{N}(0, 0.1^2)$	

Table A.1. Battery Specifications